

Effects of the load size on the maximum local SAR at 7T

Gianluigi Tiberi¹, Nunzia Fontana², Riccardo Stara³, Mark Roger Symms⁴, Agostino Monorchio², Mauro Costagli¹, Laura Biagi⁵, Mirco Cosottini⁶, and Michela Tosetti⁵

¹Imago7, Pisa, PI, Italy, ²Dipartimento di Ingegneria dell'Informazione, Pisa, Italy, ³Dipartimento di Fisica, Pisa, Italy, ⁴General Electric ASL Scientist (EMEA), Pisa, Italy, ⁵IRCCS Stella Maris, Pisa, Italy, ⁶Dipartimento di Neuroscienze, Pisa, Italy

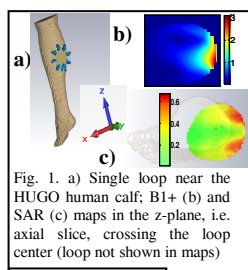


Fig. 1. a) Single loop near the HUGO human calf; B_1^+ (b) and SAR (c) maps in the z -plane, i.e. axial slice, crossing the loop center (loop not shown in maps)

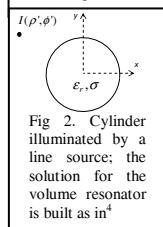


Fig. 2. Cylinder illuminated by a line source; the solution for the volume resonator is built as in⁴

Target audience. RF Engineers, Electromagnetic community in MR, researchers and clinicians interested in safety aspects at UHF.

Purpose. The evaluation of the local Specific Absorption Rate (SAR) is a major concern in ultra high field (UHF) Magnetic Resonance (MR) systems. In fact, at UHF, the energy deposition due to the radio-frequency (RF) field increases and its distribution inside the subject becomes extremely inhomogeneous and subject dependent¹. Local SAR measurements are not available in present MR systems; thus, electromagnetic simulations must be performed for RF fields and SAR analysis. In this study we resort to both 3D full wave numerical electromagnetic simulations and 2D analytical approach for investigating the dependence of the maximum local SAR at 7T with respect to the subject size, i.e. load size. It will be shown that the maximum local SAR decreases with decreasing load size: this holds true if the RF magnetic fields (B_1^+) for the different load sizes are scaled so to achieve the same B_1^+ slice average value.

Methods. Concerning the 3D full wave numerical electromagnetic simulations, we resorted to the Finite Integration Technique (FIT) in Time-Domain employed in CST MW Suite. Specifically, we simulated a single loop having radius 5 cm and positioned near the human calf extracted from the anatomic adult human model HUGO (CST MW Suite), as shown in Fig 1. The coil has been tuned to the frequency of 298 MHz and matched, achieving $s_{11} = -10$ dB (details of the tuning and matching capacitor can be found in²). RF fields

and SAR inside the calf are calculated when applying 1W of input power. The average B_1^+ magnitude calculated in the axial slice crossing the coil center is computed, together with maximum of the local SAR (10g. per unit RF cycle) calculated in the same slice. Next, we repeated the simulations using other human calves extracted from 2 anatomic adult human models (Virtual population, ITIS foundation) and 4 anatomic child models (Virtual population, ITIS foundation). In all the simulations we took particular care in keeping fixed the distance between the calves and the center of the coil (15 mm). Note the variation of the dielectric properties of tissues with the age is not considered³.

Concerning the 2D analytical approach, we resorted to a recently introduced procedure based on theory of cylindrical waves radiated by a filament of a-c current⁴ (dynamic solution). Specifically, the 16-element shielded volume resonator operating in quadrature having "bolt circle" radius of 29.5 cm and shield circle radius of 37.5 cm has been reproduced by means of line currents. A homogeneous cylindrical phantom with average tissue dielectric properties⁵ ($\epsilon_r=52$, $\sigma=0.55$ S/m) and radius 6.5 cm has been included in the simulation, as shown in Fig 2. RF fields and SAR inside the cylindrical phantom are calculated when using a feeding current of 0.1A amplitude and a frequency of 298 MHz. The average B_1^+ magnitude calculated in the cylindrical phantom is computed, together with maximum of the local SAR (per unit RF cycle) calculated in the same cylindrical phantom. Next, we repeated the simulations reducing the radius of the cylindrical phantom to 4 cm with steps of 0.25 cm. Dielectric resonance can appear for particular values of the cylindrical phantom radius, and can be determined by using the dielectric waveguides theory⁶.

Finally, we repeated the 2D analytical approach for simulating a very large volume coil, i.e. having a "bolt circle" radius of 1.295 m and shield circle radius of 1.375m.

Results and Discussions. Fig 1 show the maps of B_1^+ magnitude [μ T] and SAR [W/Kg] in the axial slice crossing the coil center obtained by using CST MW Suite with the human model HUGO. Both the maps are given only in the region occupied by the load. B_1^+ shows the typical quadropolar effect generated by a single loop; moreover, it is possible to see that the magnitude of B_1^+ decreased with depth into the calf. We noted that modification of the matching capacitor leads to a modification of the scale of both B_1^+ magnitude and SAR maps, but the shape of these maps will be not affected.

Table I summarizes the results obtained by using CST MW Suite for all the anatomic human models here used. Specifically, in the first column the details (age, gender) of the anatomic human models used to extract the calf are given; the second and the third columns show the average B_1^+ magnitude calculated in the axial slice crossing the coil center and the maximum of the local SAR calculated in the same slice. From the third column, one could conclude that the maximum SAR is higher in small size-load, i.e. in children; this is in agreement with⁷ where the SAR due to a plane wave has been investigated. However, from the second column, it is possible to note a large variability in the average B_1^+ : this variability depends on the different shape and size of the human calf models (i.e. different boundary conditions) and on the different loading (i.e. matching) conditions. The fourth and the fifth columns show the average B_1^+ magnitude and the maximum of the local SAR after scaling the simulations so to achieve the same B_1^+ slice average value of 1 μ T; after such scaling, it is possible to note that the maximum local SAR decreases if decreasing the load size, i.e. in children.

In Table II we report the results obtained by using the 2D analytical approach for analyzing cylindrical phantoms inside the volume resonator. In the first column the radius of the cylindrical phantoms is given in descended order; the second and the third columns show the average B_1^+ magnitude and the maximum of the local SAR calculated in the same cylindrical phantom. The fourth and fifth columns show the average B_1^+ magnitude and the maximum of the local SAR after scaling the simulations so to achieve the same B_1^+ average value of 1 μ T; after such scaling, it is possible to note that the maximum local SAR decreases almost monotonically if decreasing the radius.

To be sure that such decreasing is not related to the proximity effects between the load and the line currents representing the volume resonator, we repeated the 2D analytical simulation for a very large volume coil obtaining the same results (relative difference in the scaled maximum local SAR < 1%).

It should be noted that the monotonical behavior of the maximum local SAR decreasing is slightly interrupted for radius equal to 5.75 cm and 4.75: these values correspond to cylindrical phantom dielectric resonances.

Conclusion. The effect of the load size on the maximum local SAR at 7T has been analyzed. Specifically, we resorted to: i) 3D full wave numerical electromagnetic simulations for analyzing a surface loop loaded with anatomic human calves models; ii) 2D analytical approach for analyzing a volume resonator loaded with homogeneous cylindrical phantoms having average tissue dielectric properties. In both cases we noticed that the maximum local SAR decreases if decreasing the load size: this holds true if the RF magnetic fields (B_1^+) for the different load sizes are scaled so to achieve the same slice average value of 1 μ T. Obviously, we can scale the simulations so to achieve an arbitrary B_1^+ slice average value (rather than 1 μ T) or an arbitrary average flip angle; this is quite similar to what conventional *autoprescan* routines do. In any case, the same trend here discussed will hold.

References. [1] CM Collins et al. MRM, 1998;40,846-56. [2] R Stara et al., PIER M, 2013; 29, 121-136. [3] PA Hagsall et al, IT'IS Database for thermal and electromagnetic parameters of biological tissues, V. 2.4, July 30th, 2013. [4] G. Tiberi et al, JMR, 2013; 230,186-197. [5] X Zhang X et al, ISMRM 2013, p 4429. [6] RF Harrington, Time-Harmonic Electromagnetic Fields, 1961, McGraw-Hill Book Company. [7] E Conil E et al. Phys Med Biol., 2008; 53 (6): 1511-25

TABLE I (B_1^+ is in μ T, SAR in W/Kg)

	avg(B_1^+)	max SAR	avg(B_1^+) after scaling	max SAR after scaling
Hugo, M, adult	0.52	0.68	1	2.51
Duke, M, 34	0.65	1.03	1	2.43
Ella, F, 26	0.68	0.93	1	2.02
Billie, F, 11	1.04	1.29	1	1.19
Dizzy, M, 8	1.32	2.10	1	1.20
Thelonus, M, 6	1.37	1.89	1	1.01
Roberta, F, 5	1.46	1.72	1	0.80

TABLE II (B_1^+ is in μ T, SAR in W/Kg)

	avg(B_1^+)	max SAR	avg(B_1^+) after scaling	max SAR after scaling
r= 6.5 cm	0.94	2.10	1	2.37
r= 6.25 cm	1.01	2.38	1	2.29
r= 6 cm	1.11	2.72	1	2.20
r=5.75 cm	1.15	3.12	1	2.35
r=5.5 cm	1.27	3.58	1	2.20
r=5.25 cm	1.41	4.07	1	2.04
r= 5 cm	1.54	4.50	1	1.87
r= 4.75 cm	1.58	4.78	1	1.89
r= 4.5 cm	1.68	4.80	1	1.70
r=4.25 cm	1.73	4.55	1	1.51
r=4 cm	1.74	4.07	1	1.33